# A Wavelet Scattering Convolutional Network for Magnetic Resonance Spectroscopy Signal Quantitation

Amirmohammad Shamaei[1,2][a], Jana Starčuková[1][b] and Zenon Starčuk Jr.[1][c]

[1]*Institute of Scientific Instruments of the CAS, Královopolská 147, 612 64 Brno, Czech Republic*
[2]*Department of Biomedical Engineering, Faculty of Electrical Engineering and Communication, Brno University of Technology, Technická 3058/10, 616 00 Brno, Czech Republic*

Keywords: Magnetic Resonance Spectroscopy, Quantification, Deep Learning, Machine Learning.

Abstract: Magnetic resonance spectroscopy (MRS) can provide quantitative information about local metabolite concentrations in living tissues, but in practice the quantification can be difficult. Recently deep learning (DL) has been used for quantification of MRS signals in the frequency domain, and DL combined with time-frequency analysis for artefact detection in MRS. The networks most widely used in previous studies were Convolutional Neural Networks (CNN). Nonetheless, the optimal architecture and hyper-parameters of the CNN for MRS are not well understood; CNN has no knowledge about the nature of the MRS signal and its training is computationally expensive. On the other hand, Wavelet Scattering Convolutional Network (WSCN) is well-understood and computationally cheap. In this study, we found that a wavelet scattering network could hopefully be also used for metabolite quantification. We showed that a WSCN could yield results more robust than QUEST (one of quantitation methods based on model fitting) and the same as a CNN while being faster. We used wavelet scattering transform to extract features from the MRS signal, and a superficial neural network implementation to predict metabolite concentrations. Effects of phase, noise, and macromolecules variation on the WSCN estimation accuracy were also investigated.

## 1 INTRODUCTION

Magnetic Resonance Spectroscopy (MRS) has attracted the MR community over the past seven decades (Van Der Graaf, 2010). A significant part of the interest in biomedical MRS stems from the possibility of noninvasive measurements of metabolites. Information about tissue metabolites can help in clinical diagnostics. For instance, detection of metabolic pathway changes may facilitate diagnosing disease in earlier stages before anatomy changes can be observed, and thus enable more efficient treatment. E.g., in glioma, a decrease of N-acetylaspartate (NAA) and creatine concentrations and an increase of choline, lipids, and lactate predicts an increase of the glioma grade (Robin A. de Graaf, 2019; Van Der Graaf, 2010). To detect such changes, quantification of MRS signals is required for obtaining the metabolite concentrations in the tissue. However,

reliable quantification of MRS is difficult. The existing MRS quantitation methods are based on model fitting of the signal in either the time or the frequency domain (Poullet et al., 2008). In recent years, new novel machine learning solutions have been proposed for quantification, one of which is deep learning (DL). Even though the first usage of machine learning dates back to the 1970s, it was unpractical until the past decade due to lack of high-performance hardware and novel algorithms (Chen et al., 2020). DL has achieved many accomplishments in a wide range of tasks, including the MRI field (Alaskar, 2019). Due to the poor SNR, chemical shift displacement, and overlapping signal components in MRS signals, only recently has DL been used for metabolite quantification of MRS signals in the frequency domain (Hatami et al., 2018; Lee & Kim, 2019)

[a] https://orcid.org/0000-0001-8342-3284
[b] https://orcid.org/0000-0003-0337-7893
[c] https://orcid.org/0000-0002-1218-0585

Hatami et al. showed the first step in this area by using the Convolutional Neural Network (CNN) approach for simulated MRS signal quantification (Hatami et al., 2018). Kim et al. conducted a comprehensive study on brain metabolite quantification using DL (Lee and Kim, 2019). Nonetheless, the practical application of DL in MRS has not been limited to quantifications only. Kyathanahally et al. taught a CNN with time-frequency data to detect and remove ghosting artifacts in clinical magnetic resonance spectra of the human brain (Kreis & Kyathanahally, 2018).

However, the optimal architecture and hyper-parameters of CNN for MRS are not well understood. Besides, training a CNN is a computationally expensive and time-consuming task, and it usually needs a big dataset (Bruna & Mallat, 2013). Moreover, in the case of MRS signals, CNN has no understanding of the nature of the signal, and therefore, any shape difference of the signal under investigation from signals in the training data set can lead to CNN failure. If we look at a CNN as a transformation from the time domain to a features domain, due to the nature of MRS signals, the transformation should be invariant to time shift, deformation in the time domain, and frequency shift. To satisfy such requirements, CNN could be designed as

- an optimized and simple deep architecture which pools the features using a nonlinear averaging measure.

- a network with a fast computational algorithm which is stable to time-shifting, deformation in the time domain, and frequency shift.

Wavelet Scattering Convolutional Network (WSCN) can be a method of choice. WSCNs are well-understood, computationally cheap, and fast for a deep learning task (Andén & Mallat, 2014; Bruna & Mallat, 2013). Wavelet-based methods have previously been used for MRS quantification and water removal (Poullet et al., 2008; Suvichakorn et al., 2008); but as far as we are aware, wavelet transform has not been implemented by a deep convolutional neural network to quantify MRS signals.

Given the mentioned accomplishments of machine learning in MRS for signal quantification, this paper describes to our knowledge the first attempt to use this state-of-the-art technique to quantify MRS signals by WSCNs. We used wavelet scattering transform to extract features from the free induction decay (FID, i.e. the MRS signal in the time domain) and a superficial neural network implementation to predict metabolite concentrations.

In this study, we used two different basis sets. The first basis set was the ISMRM challenge 2016 simulated basis set for comparing results of our method with the results published for a CNN and another conventional quantification method, QUEST (Graveron-Demilly, 2014). For the second basis set, we simulated our own metabolite signals and generated different synthetic datasets from them for evaluating our method against phase changing, noise, and presence of macromolecule signals.

## 2 METHODS

All steps were run on a laptop with a 4-core Intel i7 processor running at 2.6 GHz and an NVIDIA GTX 1050Ti graphics processing units using Matlab (R2019a, Mathworks Inc., Natick, MA, USA) software.

### 2.1 Simulation of Metabolites

To build a basis-set signals, fifteen metabolites – Alanine (Ala), Aspartate (Asp), Creatine (Cr), Choline (Cho), Gamma Aminobutyric Acid (GABA), Glutathione (GSH), Glutamine (Gln), Glutamate (Glu), Lactate (Lac), N-Acetylaspartate (NAA), N-acetyl-aspartyl-glutamate (NAAG), Phosphatidyl-choline (PC), Phosphocreatine (PCr), Taurine (Tau) and myo-Inositol (mIns) – were simulated at 9.4 T magnetic field with the PRESS sequence (TE = 20 ms; TR = 2500 ms; acquisition points: 2048; acquisition bandwidth: 4401.41 Hz; three PRESS pulses with Hermite shapes and flip angles: P1 = 90°, P2 = 180°, P3 = 180°). The simulation was performed in NMRScopeB (Starčuk & Starčuková, 2017; Stefan et al., 2009). The parameters selected in the sequence were taken from an *in-vivo* experiment, which allows reusing the simulated basis set.

### 2.2 Baseline and Macromolecule Simulation

The baseline signals were simulated as a linear combination of several Gaussian lines identified by Osorio-Garcia (Opstad et al., 2008; Osorio-Garcia et al., 2011). The number and parameters of Gaussian lines were extracted from in-vivo signals using inversion recovery (Osorio-Garcia et al., 2011).

### 2.3 Signal Generation Framework

The MRS signal was defined as a linear combination

of amplitude-scaled frequency- and phase-shifted metabolite signals, the baseline, and noise.

The model describing a time-domain MRS signal $s[n]$ as a combination of several metabolite profiles is (Poullet et al., 2007):

$$s[n] = \sum_{m=1}^{M} A_m \, X_m[n] \, e^{(\Delta\alpha_m + i2\pi\Delta f_m)n\Delta t} \, e^{i\Delta\theta_m} +$$
$$+ A_{MM} \, MM[n] e^{(\Delta\alpha_{MM} + i2\pi\Delta f_{MM})n\Delta t} \, e^{i\Delta\theta_{MM}} + \qquad (1)$$
$$+ \varepsilon[n]$$

where $X_m[n]$ is the $n$-th sample of the $m$-th simulated metabolite, $\Delta T$ is the sampling period, $A_m$ is the scaling factor of the metabolite, $\Delta\alpha_m$ is the damping factor, $\Delta f_m$ is the frequency shift of the $m$-th metabolite affected by the static magnetic field inhomogeneity, pH, temperature and chemical composition of the tissue, $\Delta\theta_m$ is the phase of the $m$-th metabolite, $\Delta t$ is the time step, and $M$ is the number of metabolites.

Table 1 specifies the range of parameter values used for generating different datasets according to equation (1). For a comparison of our results with the previous study (Hatami et al., 2018), the basis set provided for the ISMRM challenge 2016 (ISMRM, 2016) was used to generate dataset DSS1 (20 metabolite and one macromolecule components). All other datasets were generated using the basis set simulated with NMRScopeB (15 metabolites). The same parameter ranges that were used in the previous study (Hatami et al., 2018) were also used in this study for DSS1, but we decided to choose ranges of parameters for other datasets (DSS2-DSS7) in the same manner as we would do if we evaluated real acquired spectra.

Instead of generating 500 000 signal samples per dataset, in our study only 10 000 signal samples were generated for validating the hypothesis that our network is as robust as Hatami et al.'s approach (Hatami et al., 2018) even with a smaller number of samples but faster. Parameters were chosen randomly from defined ranges with a uniform distribution. In DSS1, random complex Gaussian noise was added to signal samples based on the previous study (Hatami et al., 2018). In the rest of the datasets, the SNR of the signal samples was adjusted by adding random noise such that the SNR was in the range of ~5 to ~15. In this study, we used MATLAB built-in snr function which calculates the signal-to-noise ratio (SNR) of an MRS signal by computing the ratio of its summed squared magnitude to that of the noise. In Table 1, the presence of a parameter is marked by a tick and the absence of a parameter by a cross.

## 2.4 Deep Learning

### 2.4.1 Invariant Wavelet Scattering Network

Invariant wavelet scattering network is a transform from the time domain to the features domain, which has three stages, namely, Convolution (wavelet), Non-linearity, and Averaging (scaling factor).

In contrast to the classical wavelet transform, the Complex wavelet transform is translation invariant. In this study, we chose Morlet (Gabor) wavelets, a type of complex wavelet transform, because they have a simple mathematical representation.

Figure 1 illustrates the wavelet scattering transform processes (see (Andén & Mallat, 2014; Bruna & Mallat, 2013) for more details). In practice, a scattering decomposition framework was created with a signal input length of 1024 samples.

Table 1: Specification of datasets.

| Name | Amplitude ($A_m$) | Frequency shift($\Delta f_m$) | Damping range($\Delta\alpha_m$) | Noise ($\epsilon$) | Phase ($\Delta\theta_m$) | | MM ($A_{MM}$) | |
|---|---|---|---|---|---|---|---|---|
| | | | | | Common | Separated | Constant | Changing |
| DSS1 (Hatami et al., 2018) | [0, 1] | [-10, 10] | [-10, 10] | ✓ | ✗ | ✗ | ✗ | ✓ |
| DSS2 | [0.5 1] | [-10, 10] | [-5, 2.5] | ✗ | ✗ | ✗ | ✗ | ✗ |
| DSS3 | [0.5 1] | [-10, 10] | [-5, 2.5] | ✗ | $[-\frac{\pi}{8}, \frac{\pi}{8}]$ | ✗ | ✗ | ✗ |
| DSS4 | [0.5 1] | [-10, 10] | [-5, 2.5] | ✗ | ✗ | $[-\frac{\pi}{8}, \frac{\pi}{8}]$ | ✗ | ✗ |
| DSS5 | [0.5 1] | [-10, 10] | [-5, 2.5] | ✓ | $[-\frac{\pi}{8}, \frac{\pi}{8}]$ | ✗ | ✗ | ✗ |
| DSS6 | [0.5 1] | [-10, 10] | [-5, 2.5] | ✓ | ✓ | ✗ | ✓ | ✗ |
| DSS7 | [0.5 1] | [-10, 10] | [-5, 2.5] | ✓ | ✓ | ✗ | ✗ | Within ±10 percent of initial values |

The framework had two filter banks; in other words, the depth of the framework was 3. The quality factor (the number of wavelet filters per octave) of the first and second filter banks were 8 and 1, respectively. For the given signal length and quality factors, the output of the framework was a matrix with a size of 154 by 8 by 2. There were 154 scattering paths and 8 scattering windows for each of the real and imaginary parts of the signal.
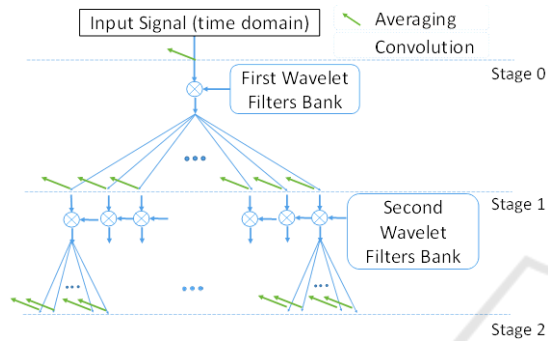
### 2.4.2 Regression



Figure 1: The process of wavelet scattering network; averaging and convolution of a signal with wavelet filters are showed by an arrow (green) and a circled star, respectively.

Flattening and fully-connected layers were what we had at the last stage of our network. The first step, so-called flattening, was converting a feature matrix into a 1-dimensional array. The matrices from the output of WSCN were flattened to create a single long feature vector. The flattening layer was connected to a fully-connected layer, which was a feedforward artificial neural network for the regression task. Neural networks with the different number of neurons in hidden layers were investigated. The best fully-connected layer structure was obtained by trial and error on the basis of the lowest error on the training and validation dataset. The results showed that one hidden-layer network with 20 neurons in the hidden layer yielded better results than other network types. The modeling performance and training were evaluated by the mean square error (MSE) and scaled conjugate gradient, respectively.

Figure 2 demonstrates the process of transformation, flattening, and regression. The input and output of a fully-connected layer were the features vector and the relative amplitudes of various metabolite basis spectra, respectively.
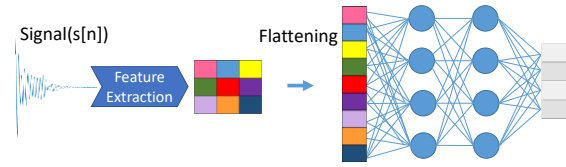


Figure 2: A schematic of feature extraction and flattening and the training of an artificial neural network.

### 2.4.3 Quantification

80% of each dataset was allocated to the training set, 10% for validation and the rest 10% for the test set. It applied to all datasets, DSS1 to DSS7, and then they were fed to the network. First, the network was trained with the training dataset; then, it was used to predict the test dataset. The output of the network was a vector in which each element represents the relative amplitude of each metabolite.

## 2.5 Accuracy Evaluation

The Symmetric mean absolute percentage error (SMAPE) is used to measure the accuracy of the model. SMAPE is defined as below for each metabolite:

$$\text{SMAPE}[m] = \frac{\sum_{n=1}^{N}\left|A_{mn} - A_{mn}^{'}\right|}{\sum_{n=1}^{N}\left(A_{mn} + A_{mn}^{'}\right)} \quad (2)$$

Where m, $N$, $A$, and $A^{'}$ are the metabolite index, the number of test datasets, the ground truth, and the estimated amplitude, respectively.

## 3 RESULTS

### 3.1 Comparison between the Quantification Result of QUEST, CNN, and WSCN for ISMRM Challenge Dataset

Figure 3 shows the comparison between different methods, namely Quest, CNN, and WSCN, for dataset DSS1, where the SNR of signals was set to 10. The result for CNN and QUEST were extracted from (Hatami et al., 2018).
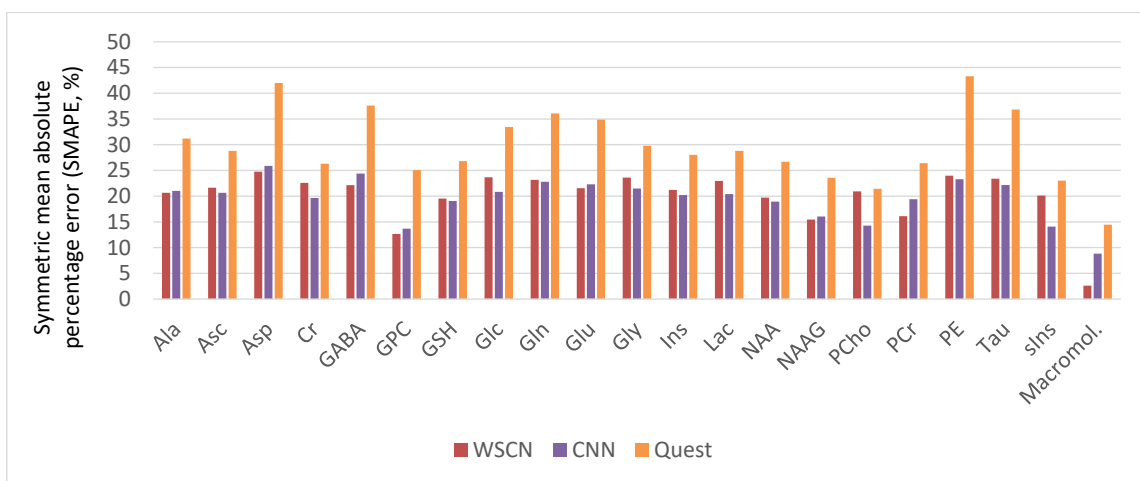
Figure 3: Comparison between SMAPEs of each metabolite for the WSCN (red), the CNN (yellow), and Quest (green).
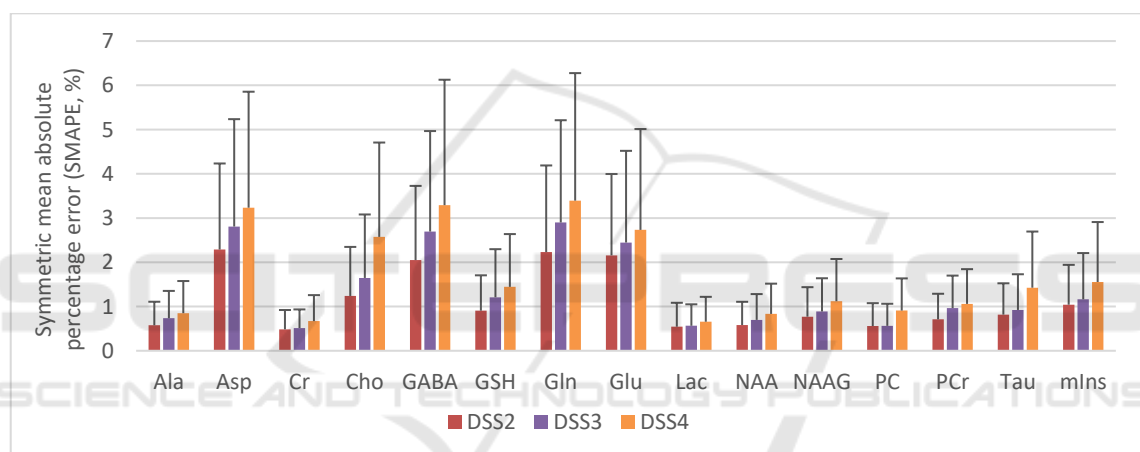


Figure 4: Comparison between SMAPEs of the concentration of all metabolites with fixed phases (DSS2), common phase varied (DSS3) and independently varied phases (DSS4) (different phase changes for different metabolites). (Test datasets, N=1000). The error bars represent the standard deviation.

## 3.2 Effect of Phase Variation and Noise on WSCN Estimation Accuracy

The performance of WSCN was evaluated on different datasets (DSS2 to DSS7) in table 1. Figure 4 shows the effect of metabolite phase variation in the signals under test. We compared the result of signals with a fixed phase, a common varied phase, and independently varied phases. The average of SMAPEs for DSS2, DSS3, and DSS4 were 1.13%, 1.38%, and 1.7%, respectively.

The results of the metabolite quantification for DSS5 (DSS3 with added noise) is shown in Figure 5. For all 15 metabolites, the average of SMAPE was $3.46\% \pm 2.81\%$. Asp with SMAPE of $6.00 \pm 4.48$ and NAAG with SMAPE of $13.20\% \pm 10.12\%$ were quantified as highest and lowest SMAPE,

respectively. The average SMAPE of DSS5 was increased by 151% compared to DSS3 (without noise).

## 3.3 Effect of Macromolecules Variation on WSCN Estimation Accuracy

Figure 6 shows a comparison between DSS6 and DSS7. In dataset DSS6, the parameters of baseline signals (11 Gaussian lines) are constant, while in DSS7, amplitudes of Gaussian lines were randomly varied in the range of ±10% of their initial values. For all metabolites of DSS6 and DSS7, the average SMAPEs were $5.92\% \pm 4.40\%$ and $6.12\% + 4.55\%$, respectively. The average SMAPE of DSS6 and DSS7 was increased by 73% compared to DSS5 (without Macromolecules inclusion).
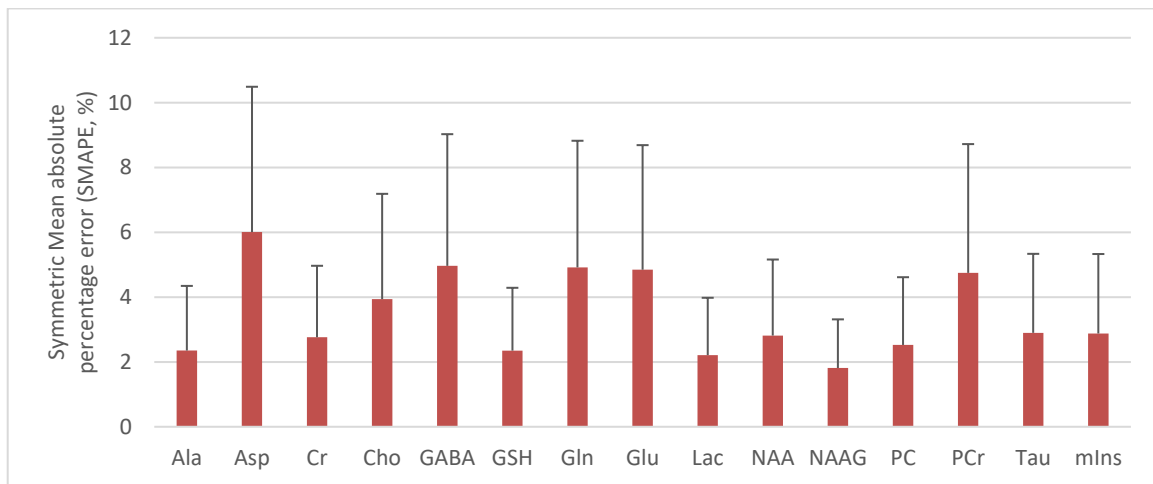
Figure 5: Symmetric mean absolute percent error (SMAPE) of the concentrations of all metabolites in dataset DSS5, which contains noisy signal (N = 5000). The error bars represent the standard deviation.
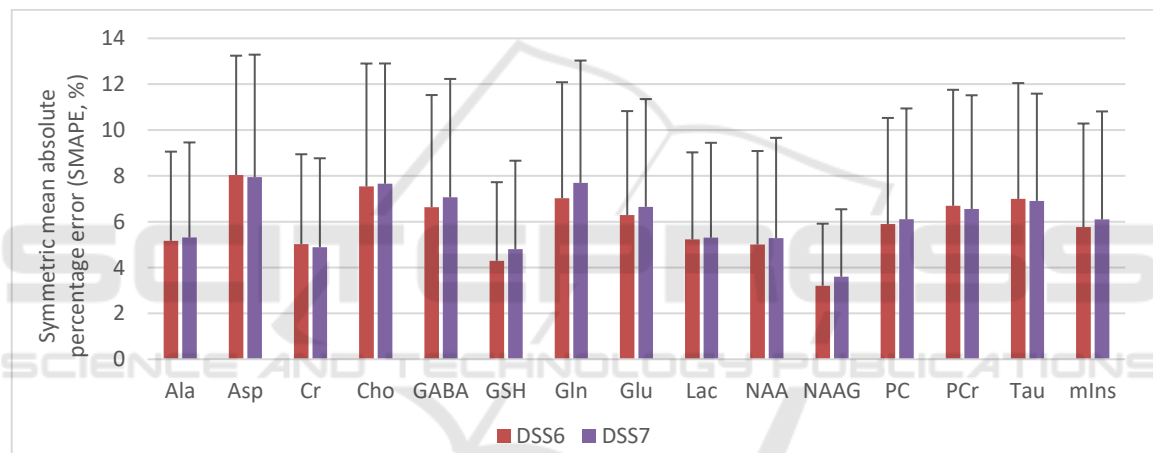


Figure 6: Comparison between SMAPEs of the concentration of all metabolites in dataset DSS6, and DSS7 (Test datasets, N=1000). In DSS6, the amplitudes of macromolecules lines were constant. In contrary, the amplitudes were varying within ±10% of initial range in DSS7. Both datasets are noisy and with common phase changing.

## 4 CONCLUSIONS

The aim of MRS signal quantification is to estimate the amplitudes/areas (in time/frequency domain) of different metabolites in the signal. The estimated amplitudes/areas then can be converted to meaningful numbers as the concentration of metabolites. The conventional and widely used approach is to estimate amplitudes of single sinusoids (areas of single peaks) in MRS signal or to estimate the amplitudes (areas) of whole metabolite signals (spectra). In the former approach, the model is fitted to data using non-linear least-squares analysis; the latter approach uses a basis set of metabolite profiles in the model function and uses a semi-parametric fitting technique. The oldest

method, so-called peak integration, is calculating peaks area in a selected frequency interval. Nonetheless, using these approaches for quantification is challenging (Stagg & Rothman, 2014).

On the other hand, the quantification of the MRS signal using deep learning has attracted huge interest in recent years (Chen et al., 2020). DL can detect important features in the MRS signal and subsequently determine a non-linear mapping between these features and the outputs, which can be the concentrations of the metabolites. The most widely used DL approach for quantification is CNN. Nevertheless, this approach has drawbacks, for example, poor understanding of the CNN architecture and hyper-parameters for MRS, expensive and time-

consuming computation, and the need of a big dataset for CNN training (Bruna and Mallat, 2013).

These shortages motivated us to develop a deep network for MRS signal quantification, which can be fast, well-understood, and works with a small dataset of training samples. For this purpose, we used a WSCN.

In every DL task, determining the proper input and output of the network is an important step. In our study, the input is an FID, i.e., time-domain signal, and the network estimates amplitudes of the first points of metabolite signals (what corresponds to areas under metabolite signals in metabolite spectra). In this work, we demonstrated that the use of the wavelet scattering network could achieve better results than the semi-parametric fitting technique QUEST and similar results as the computationally more demanding CNN (Figure 3).

It is known that the accuracy of estimation in the peak integration approaches is influenced by phases of peaks (Stagg & Rothman, 2014), and that phase should be included in the model as one of the unknown parameters. Therefore, we also investigated whether WSCN is capable of estimating amplitudes of metabolites in case that metabolite phases change. It resulted in an increase in the complexity of the model, but WSCN proved to have the capability of handling this task. Figure 4 shows the WSCN can quantify signals with common varied phases (with SMAPE of 1.38%) as well as signals without fixed phases (with SMAPE of 1.13%). The average of MAPEs for DSS4 is increased by 36% and 17% compared to DSS2 and DSS3, respectively. It indicates that quantification can be moderately harder for a dataset with independently varied phases.

Another source of error in quantification are macromolecular signals, which stem in macromolecules present in the tissue under investigation. In conventional quantification approaches, macromolecule signals can either be removed in the preprocessing step or modeled in the quantitation step. However, the risk of errors will be increased and accumulated in fitting error in the former approach, and therefore the latter approach is recommended. However, macromolecule signals often overlap with metabolite components, for which DL can be a method of choice for disentangling. As we showed in Figure 3, the WSCN could estimate macromolecules better than other approaches. Later in this study, we modeled the macromolecules signal as a set of Gaussian lines using parameters (like linewidth, frequency) measured using the inversion-recovery recovery (Osorio-Garcia et al., 2011). Figure 6 demonstrates that the WSCN showed nearly the same error for signals with randomly varied macromolecule lines and signals with fixed macromolecule lines. This could indicate that despite the changing of background signals parameters, the WSCN is stable against nuisance components in MRS, such as macromolecules. Additional research should be done however with simulated signals that will imitate *in-vivo* data.

To compare the learning times of both networks, i.e., Hatami et al.'s CNN and our WSCN, we rebuilt their CNN and fed both networks with the DSS5 dataset, and ran both networks in the earlier mentioned system. Our proposed approach is estimated to be 45 times faster than Hatami et al.'s approach (the WSCN's learning time was 5 min 40 sec precisely and the CNN's learning time was 268 min). The WSCN showed that it could be faster than the CNN due to using fixed-size filters and less parameter optimization.

It should be noted that even though deep learning showed promising results in areas like speech recognition and image processing (Chen et al., 2020), this study is one of the very initial steps in the application of DL in MRS and more studies are needed for proving DL suitability for *in-vivo* spectroscopy. Below some of the limitations and open issues are addressed:

1. In this study, we only quantified simulated data. The amplitudes of metabolites in our simulated data did not imitate the metabolite concentrations in *in-vivo* data. Quantification of simulated data with concentrations close to *in-vivo* data should be investigated as the next step together with data acquired from a phantom.

2. Real MRS data is influenced by numerous factors such as voxel size, voxel placement, radiofrequency (RF) coil sensitivity, receiver gain, and other experimental factors. Further research must take all factors into account.

3. A potential application of our proposed approach is the quantification of MRSI data, where a fast method is needed for quantification of a set of MRS signal. Learning a network and using it for only a single voxel may not be efficient as using it for a set of signals.

## ACKNOWLEDGEMENTS

infrastructure for biological and medical imaging" of the Ministry of Education, Youth and Sports of the CR (No. CZ.02.1.01/0.0/0.0/16_013/0001775).

# REFERENCES

Alaskar, H. (2019). *Deep Learning-based Model Architecture for Time-Frequency Images Analysis*. *January 2018*.

Andén, J., & Mallat, S. (2014). Deep scattering spectrum. *IEEE Transactions on Signal Processing*, *62*(16), 4114–4128.

Bruna, J., & Mallat, S. (2013). Invariant scattering convolution networks. *IEEE Transactions on Pattern Analysis and Machine Intelligence*, *35*(8), 1872–1886.

Chen, D., Wang, Z., Guo, D., Orekhov, V., & Qu, X. (2020). Review and Prospect: Deep Learning in Nuclear Magnetic Resonance Spectroscopy. *Chemistry - A European Journal*, *26*(46), 10391–10401.

Graveron-Demilly, D. (2014). Quantification in magnetic resonance spectroscopy based on semi-parametric approaches. In *Magnetic Resonance Materials in Physics, Biology and Medicine* (Vol. 27, Issue 2, pp. 113–130). Springer Verlag.

Hatami, N., Lyon, B., & Etienne, U. (2018). *Magnetic Resonance Spectroscopy Quantification using Deep Learning*.

ISMRM. (2016). *MRS Fitting Challenge (ismrm.org /workshops/Spectroscopy16/mrs_fitting_challenge/)*.

Kreis, R., & Kyathanahally, S. P. (2018). *Deep Learning Approaches for Detection and Removal of Ghosting Artifacts in MR Spectroscopy*. *863*, 851–863.

Lee, H. H., & Kim, H. (2019). Intact metabolite spectrum mining by deep learning in proton magnetic resonance spectroscopy of the brain. *Magnetic Resonance in Medicine*, *82*(1), 33–48.

Opstad, K. S., Bell, B. A., Griffiths, J. R., & Howe, F. A. (2008). Toward accurate quantification of metabolites, lipids, and macromolecules in HRMAS spectra of human brain tumor biopsies using LCModel. *Magnetic Resonance in Medicine*, *60*(5).

Osorio-Garcia, M. I., Sima, D. M., Nielsen, F. U., Dresselaers, T., Van Leuven, F., Himmelreich, U., & Van Huffel, S. (2011). Quantification of in vivo 1H magnetic resonance spectroscopy signals with baseline and lineshape estimation. *Measurement Science and Technology*, *22*(11), 1–17.

Poullet, J. B., Sima, D. M., Simonetti, A. W., De Neuter, B., Vanhamme, L., Lemmerling, P., & Van Huffel, S. (2007). An automated quantification of short echo time MRS spectra in an open source software environment: AQSES. *NMR in Biomedicine*, *20*(5), 493–504.

Poullet, J. B., Sima, D. M., & Van Huffel, S. (2008). MRS signal quantitation: A review of time- and frequency-domain methods. *Journal of Magnetic Resonance*, *195*(2), 134–144.

Robin A. de Graaf. (2019). In Vivo NMR Spectroscopy. In *In Vivo NMR Spectroscopy* (pp. 1–42).

Stagg, C., & Rothman, D. (2014). *Magnetic Resonance Spectroscopy: Tools for Neuroscience Research*.

Starčuk, Z., & Starčuková, J. (2017). Quantum-mechanical simulations for in vivo MR spectroscopy: Principles and possibilities demonstrated with the program NMRScopeB. *Analytical Biochemistry*, *529*.

Stefan, D., Cesare, F. Di, Andrasescu, A., Popa, E., Lazariev, A., Vescovo, E., Strbak, O., Williams, S., Starcuk, Z., Cabanas, M., Van Ormondt, D., & Graveron-Demilly, D. (2009). Quantitation of magnetic resonance spectroscopy signals: The jMRUI software package. *Measurement Science and Technology*, *20*(10).

Suvichakorn, A., Ratiney, H., Bucur, A., Cavassila, S., & Antoine, J. P. (2008). Quantification method using the Morlet wavelet for Magnetic Resonance Spectroscopic signals with macromolecular contamination. *Proceedings of the 30th Annual International Conf. of the IEEE Engineering in Medicine and Biology Society, EMBS'08 - "Personalized Healthcare through Technology,"* 2681–2684.

Van Der Graaf, M. (2010). In vivo magnetic resonance spectroscopy: Basic methodology and clinical applications. *European Biophysics Journal*, *39*(4), 527–540.